COMPUTATION OF EM FIELD SCATTERED BY AN OPEN-ENDED CAVITY AND BY A CAVITY UNDER RADOME USING THE ITERATIVE PHYSICAL OPTICS

R. Hemon

Laboratoire IREENA, EA 1170, Ecole Polytechnique de Nantes
Bât. IRESTE, La Chantrerie 44306 Nantes cedex 3, France

P. Pouliguen

DGA/DET/Centre d'ELectronique de l'ARmement (CELAR)
35170 Bruz, France

H. He and J. Saillard

Laboratoire IREENA, EA 1170, Ecole Polytechnique de Nantes
Bât. IRESTE, La Chantrerie 44306 Nantes cedex 3, France

J. F. Damiens

DGA/DET/Centre d'ELectronique de l'ARmement (CELAR)
35170 Bruz, France

Abstract—It is always a challenge to predict Radar Cross Section (RCS) of a full scale military platform with a good accuracy. Most of the time antennas and cavities are the main contributors of aircrafts RCS. Several methods have been developed to compute the RCS of cavities such as analytical methods (modal methods) and asymptotic methods (geometrical optics (GO) methods and physical optics (PO) methods). This article presents the Iterative Physical Optics (IPO) method which consists in an iterative resolution of the Magnetic Field Integral Equation (MFIE) to compute the currents on the inner walls of the cavity. This method allows computing arbitrarily shaped cavity with a good accuracy even for cavity with a depth inferior to the wavelength. Comparisons of IPO results with Rays and Finite element methods show a better accuracy of IPO than Rays especially for cross polarization. But computation time represents one of the main limitations of the IPO method. We present here a new formulation of the Segmented IPO method which coupled with the

generalized reciprocity theorem decreases significantly the complexity of the method and consequently the computation time. The S-IPO method has been validated by comparisons with Modal method and measurements. We have observed that the repartition of the electric currents density on the inner walls of the cavity is quite the same with IPO and S-IPO computations. Lastly we propose an evolution of the IPO method we have developed to compute the RCS of cavities under radome. This method has been validated by comparison with finite element results.

1. INTRODUCTION

Electromagnetic signature of targets with cavities, like inlets of aircrafts and missiles, has been the subject of numerous theoretical and experimental studies [1]. Inlets of such targets contribute significantly to their Radar Cross Section (RCS). Numerical methods like Method of Moments and Finite Element Methods could be employed to analyze cavities but complexity of these methods increases with frequency and dimensions of the cavities. That's why these methods are generally not used to solve this problem. Modal methods have been developed to analyze cavities with canonical shapes [2, 3]. In other way asymptotical methods like Ray methods [5, 7, 8] or Physical Optics methods [11, 12] allow to compute RCS of relatively arbitrarily shaped cavities. The method presented here, the Iterative Physical Optics method [12–14], is one of these asymptotical methods. The first part recalls the IPO method. Some comparisons of IPO results with modal, Ray, FE methods and measurements are presented. A convergence criterion is proposed and results are showed. Then the second part, presents a new formulation of the Segmented-IPO method [15] used to increase the efficiency of IPO method with and without the use of the general reciprocity integral [6] and the convergence criterion. The last part presents an evolution of the IPO method we have developed to compute the RCS of cavities under radome [23].

2. DESCRIPTION OF THE IPO METHOD

The Iterative Physical Optics method has been developed in 1995 [12] to compute the RCS of electrically large open-ended cavities. It is an asymptotical method which consists in an iterative resolution of the Magnetic Field Integral Equation to compute the electric and magnetic currents on the inner walls of the cavity. The computation of EM field scattered to the observation point by the cavity is divided in five steps:

1. Computation of electric and magnetic equivalent currents induced by incident EM field over the aperture
2. Computation of EM fields radiated by equivalent currents over the aperture on the inner walls of the cavity
3. Iterative computation of electric and magnetic currents induced on the facets of the inner walls by EM fields radiated by equivalent currents over the aperture and by currents on the other facets of the inner walls.
4. Computation of EM field radiated by currents on the inner walls over the aperture
5. Computation of EM fields scattered at the observation point.

The notations used in all the following developments are represented in Figure 2. An $e^{-j\omega t}$ dependence is assumed and suppressed. The IPO formulation is given for a cavity with inner walls coated with dielectric materials [13, 14]. In such case Leontovitch condition [9] is applied to compute the magnetic current as a function of the electric current such as:

$$\vec{M} = Z_0 Z_s (\vec{J} \wedge \hat{n})$$

Where: Z_s is relative impedance of medium 1 (Figure 1): $Z_s = \sqrt{\dfrac{\mu_r}{\varepsilon_r}}$

$Z_0 = 120\pi$ is free space impedance
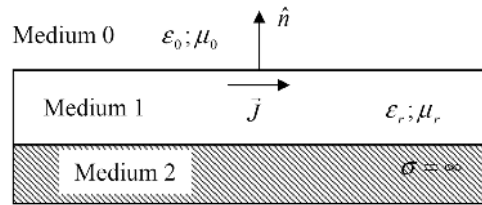
Figure 1.

Leontovitch condition could be applied when:
- $|N| = \left|\sqrt{\mu_r \varepsilon_r}\right| \gg 1$
- $|\text{Im}(N)| k\rho_{\min} \gg 1$
- $\dfrac{\nabla Z_s}{k Z_s} \ll 1$, this relation limits the application of Leontovitch condition to homogenous or weakly heterogeneous materials

Where:

N is the refraction index of Medium 1 relative to Medium 0 (free space)

k is free space wave number

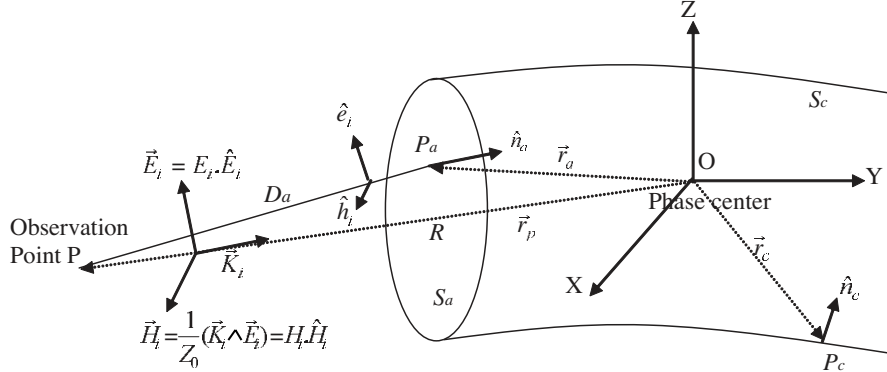$\rho_{\min}$ is the most little curvature radius of the surface between media 0 and 1.

Figure 2.

Step one: Computation of equivalent currents induced over the aperture

The EM field incident on a point of the aperture is:

$$\vec{E}_i(P_a) = E_i * G_e * \frac{e^{jkD_a}}{D_a} \hat{e}_i$$
$$\vec{H}_i(P_a) = H_i * G_e * \frac{e^{jkD_a}}{D_a} \hat{h}_i$$

$$(1)$$

Where:

D_a is the distance between the Transmitter and a point P_a over the aperture.

G_e is the transmitter gain

In the next G_e and E_i are assumed to be equal to 1 thus $H_i = \frac{1}{Z_0}$

Electric and magnetic equivalent currents induced over the aperture are given by:

$$\vec{J}_i(P_a) = \frac{\vec{n}_{Ji}}{Z_0} \frac{e^{jkDa}}{D_a}$$
$$\vec{M}_i(P_a) = \vec{n}_{Mi} \frac{e^{jkDa}}{D_a}$$

$$(2)$$

Where:

$$\vec{n}_{Ji} = \hat{n}_a \wedge \hat{h}_i$$
$$\vec{n}_{Mi} = \hat{e}_i \wedge \hat{n}_a$$

$\hat{n}_a$ is the unit vector normal to the aperture

Step two: Computation of the magnetic field induced on the inner walls of the cavity

It is computed using the Kirchhoff approximation:

$$\vec{H}_d^{S_a}(P_c) = \int\limits_{S_a} \vec{J}_i(P_a) \wedge \vec{\nabla}' G(\vec{r}_c - \vec{r}_a) dS_a$$

$$- \frac{1}{jkZ_0} \vec{\nabla} \wedge \int\limits_{S_a} \vec{M}_i(P_a) \wedge \vec{\nabla}' G(\vec{r}_c - \vec{r}_a) dS_a \qquad (3)$$

Where:

$\vec{r}_a$ and $\vec{r}_c$ are respectively points over the aperture S_a and on the inner wall S_c

$\vec{\nabla}' G$ is the gradient of the free space Green's function

Step three: Iterative computation of electric and magnetic currents induced on the inner walls

These currents are induced by radiation of equivalent currents over the aperture and currents on the other facets of the inner walls. Consequently the electric current $\vec{J}_N(\vec{r}_{c_v})$ at a point v at iteration N is given by:

$$\vec{J}_N(P_{c_v}) = \vec{J}_0(P_{c_v}) + 2\hat{n}_{c_v} \wedge \left\{ \int\limits_{S_c} \vec{J}_{N-1}(P_{c_u}) \wedge \vec{\nabla}' G(\vec{r}) dS_c \right.$$

$$\left. - \frac{1}{jkZ_0} \vec{\nabla} \wedge \int\limits_{S_c} \vec{M}_{N-1}(P_{c_u}) \wedge \vec{\nabla}' G(\vec{r}) dS_c \right\} \qquad (4)$$

Leontovitch condition is applied to give:

$$\vec{J}_N(P_{c_v}) = \vec{J}_0(P_{c_v}) + 2\hat{n}_{c_v} \wedge \left\{ \int\limits_{S_c} \vec{J}_{N-1}(P_{c_u}) \wedge \vec{\nabla}' G(\vec{r}) dS_c \right.$$

$$\left. - \frac{1}{jkZ_0} \vec{\nabla} \wedge \int\limits_{S_c} Z_0 Z_S (\vec{J}_{N-1}(P_{c_u}) \wedge \hat{n}_{c_u}) \wedge \vec{\nabla}' G(\vec{r}) dS_c \right\} \quad (5)$$

Where:

$\vec{r} = \vec{r}_{c_v} - \vec{r}_{c_u}$ is the vector between points 'u' and 'v' of the inner walls.

$\vec{r}_{c_v}$ is the vector between the phase center and the point 'v'

$\hat{n}_{c_v}$ is the unit vector normal to the surface S_c at point 'v'

The initial current on the inner walls is induced by EM field radiated by equivalent currents over the aperture. The total field is equal to the sum of incident and reflected fields on the inner walls such as:

$$\vec{J}_0(P_{c_v}) = \hat{n}_{c_v} \wedge \left(\vec{H}_i^{S_a}(P_{c_v}) + \vec{H}_r^{S_a}(P_{c_v}) \right) \tag{6}$$

Step four: Computation of EM fields radiated over the aperture

These EM fields are induced by EM fields radiated by electric and magnetic currents on the inner walls of the cavity using the Leontovitch condition:

$$
\begin{aligned}
\vec{E}_d^{S_c}(P_a) &= - \int_{S_c} Z_0 Z_S \left(\vec{J}_N(P_c) \wedge \hat{n}_c \right) \wedge \vec{\nabla}' G(\vec{r}_a - \vec{r}_c) dS_c \\
&\quad - \frac{1}{jkY_0} \vec{\nabla} \wedge \int_{S_c} \vec{J}_N(P_c) \wedge \vec{\nabla}' G(\vec{r}_a - \vec{r}_c) dS_c \\
\vec{H}_d^{S_c}(P_a) &= \int_{S_c} \vec{J}_N(P_c) \wedge \vec{\nabla}' G(\vec{r}_a - \vec{r}_c) dS_c \\
&\quad - \frac{1}{jkZ_0} \vec{\nabla} \wedge \int_{S_c} Z_0 Z_S \left(\vec{J}_N(P_c) \wedge \hat{n}_c \right) \wedge \vec{\nabla}' G(\vec{r}_a - \vec{r}_c) dS_c
\end{aligned}
\tag{7}
$$

Step five: Computation of electric field scattered outside the cavity

It is computed using the Kirchhoff approximation:

$$
\begin{aligned}
\vec{E}_d^{S_a}(P) = &- \int_{S_a} \vec{M}(P_a) \wedge \vec{\nabla}' G(\vec{r}_p - \vec{r}_a) dS_a \\
&- \frac{1}{jkY_0} \vec{\nabla} \wedge \int_{S_a} \vec{J}(P_a) \wedge \vec{\nabla}' G(\vec{r}_p - \vec{r}_a) dS_a
\end{aligned}
\tag{8}
$$

Where:

$$\vec{M}(P_a) = \vec{E}_d^{S_c}(P_a) \wedge \hat{n}_a$$
$$\vec{J}(P_a) = \hat{n}_a \wedge \vec{H}_d^{S_c}(P_a)$$

In order to increase the convergence of the solution, shadowing effects are included in Equations (3), (4) and (7). For example, in Equation (4), if the point $\vec{r}_{c_v}$ is not visible from the point $\vec{r}_{c_u}$ the contribution to the integral from the point $\vec{r}_{c_u}$ is zero. It is the same in Equations (3) and (7) between points $\vec{r}_a$ and $\vec{r}_c$. The density of facets has to be equal to 9 or 12 facets per square wavelength in order to obtain accurate results [12]. The number of iterations required to obtain a convergent result is approximately the same that the number of wave reflections in the cavity. Nevertheless the number of iterations could vary with the incident angle. Consequently it could be interesting to use a convergence criterion. With this criterion, computation time decreases. One efficient way to test the convergence of the iterative computation is to compute the total electric current on the inner walls at iteration N. Then this total current is compared with the current at the previous iteration $N - 1$. If the current variation is small the iterative process is stopped. The criterion can be written:

$$\left| 1 - \frac{J_{N-1}}{J_N} \right| \leq \delta \tag{9}$$

Where:

$$J_{N-1} = \sum_{i=1}^{N_c} \left| \vec{J}_{N-1}^i \right|$$

$$J_N = \sum_{i=1}^{N_c} \left| \vec{J}_N^i \right|$$

This method has been validated by comparison with measurements and with FEM and modal method [4] computations. Figure 4 shows the RCS of a rectangular cavity (Figure 3) with a length of 1 m, a high of 25 cm and a width of 50 cm. The RCS has been measured in an anechoic chamber and computed with the IPO method at 3.59 GHz, for an azimuth angle range from 0° to 60° with a step of 1° and a VV polarization. 8 iterations are required. There is a good agreement between measurements and IPO computation.

Then IPO results are obtained using convergence criterion and compared with measurements.
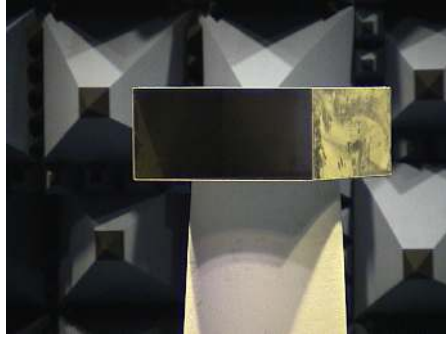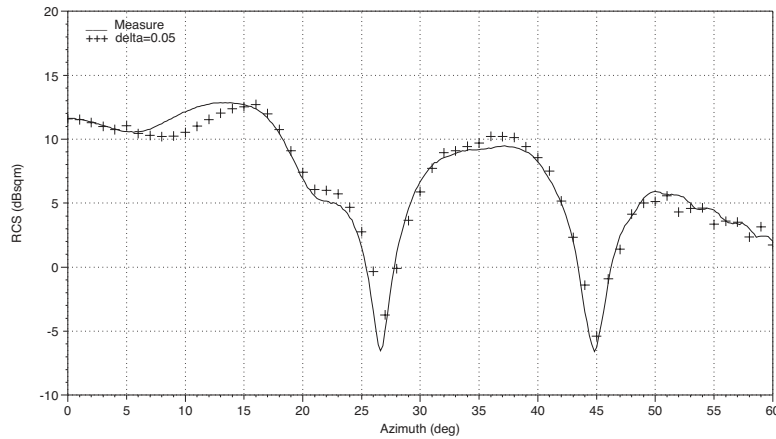
Figure 3. Rectangular cavity.
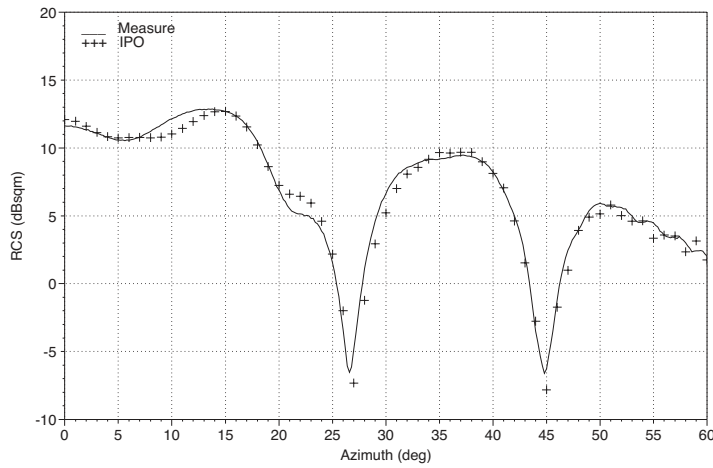
Figure 4. Comparison of IPO results with measurements. $F = 3.59\,\text{GHz}$, VV polarization, elevation angle $0°$.

Results obtained with a convergence criterion $\delta = 0.05$ are presented here (Figure 5). Computations with $\delta = 0.03$ and $\delta = 0.04$ have been performed but are not presented here. In each case there is a good agreement between measurement and IPO results. Figure 6 shows the number of iterations versus the incident angle for each convergence criterion. The number of iterations increases with the incident angle and consequently with the number of wave reflections in the cavity. For a criterion of 0.05 there is an average of 5.2 iterations and the computation time decreases.

Now, we consider a small depth cavity burrowed in a cylinder representative of cavities that are located on missile fuselage. This

Figure 5. Comparison of IPO computations using convergence criterion with measurements. $F = 3.59\,\text{GHz}$, VV polarization, elevation angle $0°$.
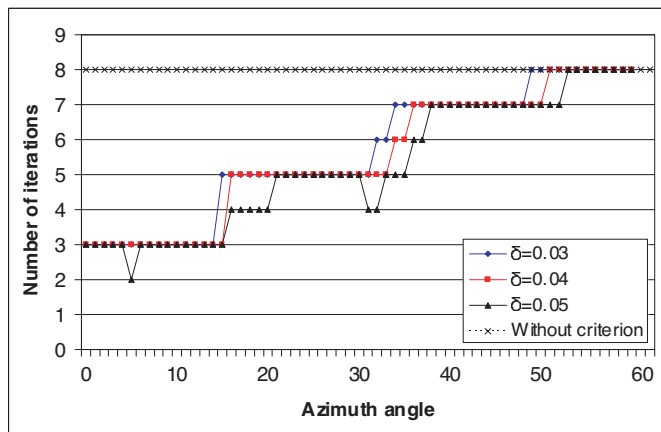
**Figure 6.** Number of iterations versus incident angle.

cavity (Figure 7) has an aperture with a size of $15\,\text{cm} * 7.5\,\text{cm}$ and a depth of $2.5\,\text{cm}$ at a maximum. It is placed on a cylinder of diameter $30\,\text{cm}$ and a length of $30\,\text{cm}$. Computations have been made at $9.2\,\text{GHz}$, for an azimuth angle range from $0°$ to $60°$ with a step of $1°$ and a VV polarization.

We observe Figure 8 a good agreement between IPO computation and measurements showing that IPO is efficient even for cavities with
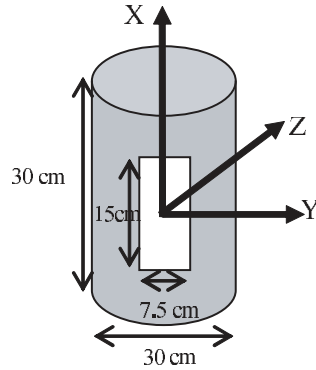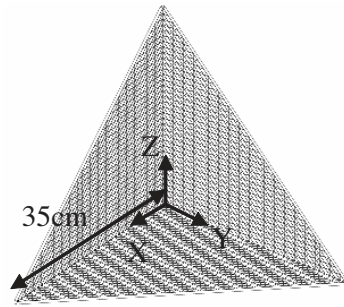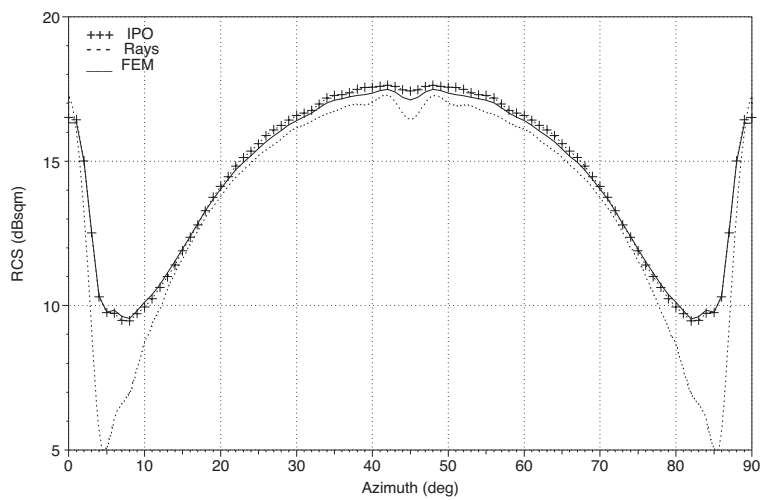
Figure 7.

depth inferior to wavelength.
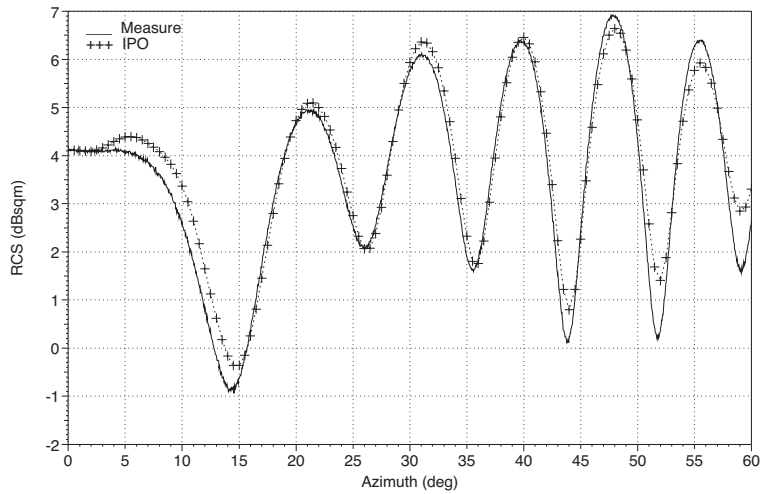
Figure 8. Comparison of IPO results with measurements. $F = 9.2\,\mathrm{GHz}$, VV polarization, elevation angle $0°$.

Then RCS of a triangular trihedral corner reflector (Figure 9) computed with a Finite Element (FE), a ray and the IPO methods have been compared. The RCS is calculated at $9\,\mathrm{GHz}$, for an azimuth angle range from $0°$ to $90°$ with a step of $1°$, an elevation angle of $35.26°$ and in VV and VH polarizations.

We observe Figure 10 and Figure 11 that IPO results are more accurate that results from the ray method in comparison with FE

Figure 9. Triangular trihedral corner reflector.

Figure 10. Comparison of IPO, Ray and FE methods in VV polarization. $F = 9\,\mathrm{GHz}$, elevation angle $35.26°$.

method. The main differences are obtained for the VH polarization Figure 11. There are about $5\,\mathrm{dB}$ differences between the ray method result and the FEM.

The precedent results show the accuracy of the IPO method. Nevertheless one of the principal problems of the IPO method is the complexity and consequently the computation time. Number of facets increases with the frequency and the dimensions of the target. That is why several studies have been made to improve the efficiency of IPO method [15–22]. One of them is based on a segmentation principle, the S-IPO method [15].
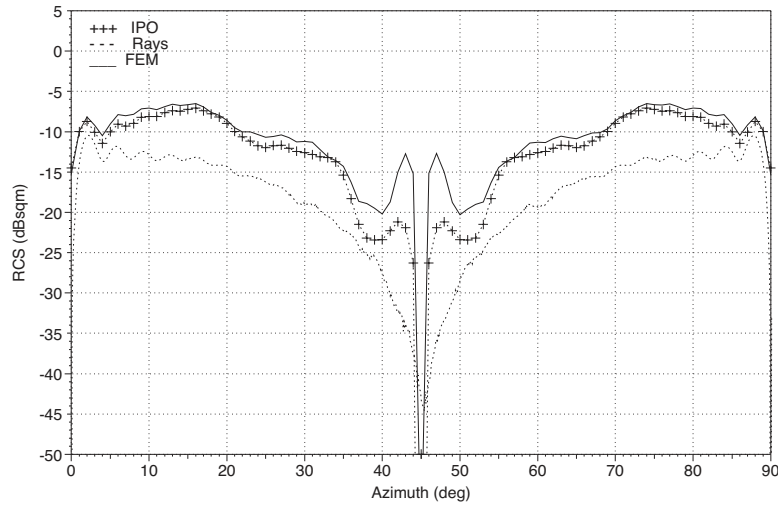
Figure 11. Comparison of IPO, Ray and FE methods in VH polarization. $F = 9\,\mathrm{GHz}$, elevation angle $35.26°$.

3. THE SEGMENTED IPO METHOD

The S-IPO method [15] consists in a decomposition of the cavity in N sections which are separated by exchange surfaces (Figure 12). The method was initially developed using S parameters. Here we propose a different approach by exchanging equivalent currents on each interface.
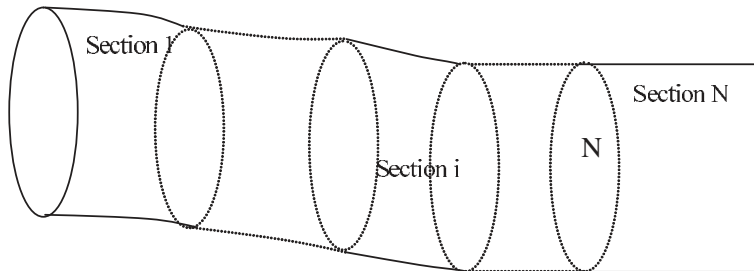
Figure 12. Segmentation of the cavity.

Each section is analyzed independently from the rest of the cavity from Section 1 to Section N. The process to analyze the section 'i' is the following:

Step one: Computation of equivalent currents on exchange

surface 'i':

The electric and magnetic equivalent currents on the exchange surface 'i' are induced by EM fields radiated by the electric and magnetic currents on the inner walls of the section '$i-1$' and by the equivalent currents on the exchange surface '$i-1$'. They are expressed:

$$\vec{M}_{Sa_i}(P_i) = (\vec{E}_d^{Sc_{i-1}}(P_i) + \vec{E}_d^{Sa_{i-1}}(P_i)) \wedge \hat{n}_a^i$$
$$\vec{J}_{Sa_i}(P_i) = \hat{n}_a^i \wedge (\vec{H}_d^{Sc_{i-1}}(P_i) + \vec{H}_d^{Sa_{i-1}}(P_i)) \tag{10}$$

Where:

$\vec{E}_d^{Sc_{i-1}}(P_i)$ and $\vec{H}_d^{Sc_{i-1}}(P_i)$ are EM fields radiated by electric and magnetic currents on the inner walls of the section '$i-1$'

$\vec{E}_d^{Sa_{i-1}}(P_i)$ and $\vec{H}_d^{Sa_{i-1}}(P_i)$ are EM fields radiated by electric and magnetic equivalent currents on the exchange surface '$i-1$'

Step two: Computation of magnetic field radiated on the inner walls of Section i

It is computed using the Kirchhoff approximation and an equation with the same form as relation (3).

Step three: Iterative computation of electric and magnetic currents on the inner walls

We compute iteratively the electric currents on the inner walls of the section 'i' by using equations with the same form as relations (4) and (5)

Step four: Computation of equivalent currents on exchange surface 'i + 1'

First the EM fields radiated by the equivalent currents on the exchange surface 'i' are computed:

$$\vec{E}_d^{Sa_i}(P_{i+1}) = -\int_{Sa_i} \vec{M}_{Sa_i}(P_i) \wedge \vec{\nabla}'G(\vec{r}_i)dSa_i$$
$$-\frac{1}{jkY_0}\vec{\nabla} \wedge \int_{Sa_i} \vec{J}_{Sa_i}(P_i) \wedge \vec{\nabla}'G(\vec{r}_i)dSa_i$$
$$\vec{H}_d^{Sa_i}(P_{i+1}) = \int_{Sa_i} \vec{J}_{Sa_i}(P_i) \wedge \vec{\nabla}'G(\vec{r}_i)dSa_i \tag{11}$$
$$-\frac{1}{jkZ_0}\vec{\nabla} \wedge \int_{Sa_i} \vec{M}_{Sa_i}(P_i) \wedge \vec{\nabla}'G(\vec{r}_i)dSa_i$$

Where: $\vec{r}_i = \vec{r}_{a_{i+1}} - \vec{r}_{a_i}$ is the vector between two points of exchange surfaces '$i+1$' and 'i'

Then the EM fields $\vec{E}_d^{Sc_i}(P_{i+1})$ and $\vec{H}_d^{Sc_i}(P_{i+1})$ radiated by electric and magnetic currents on the inner walls of the section 'i' to the exchange surface '$i+1$' are computed using relation of the form of Equation (7).

Finally the equivalent currents on exchange surface '$i+1$' are given by:

$$\begin{aligned}
\overrightarrow{M}_{Sa_{i+1}}(P_{i+1}) &= (\vec{E}_d^{Sc_i}(P_{i+1}) + \vec{E}_d^{Sa_i}(P_{i+1})) \wedge \hat{n}_a^i \\
\overrightarrow{J}_{Sa_{i+1}}(P_{i+1}) &= \hat{n}_a^i \wedge (\vec{H}_d^{Sc_i}(P_{i+1}) + \vec{H}_d^{Sa_i}(P_{i+1}))
\end{aligned} \tag{12}$$

The same method is applied, till the currents on the inner walls of the last section 'N' are computed. Then the same principle could be applied from the last to the first section, and finally the Kirchhoff approximation is used to compute EM fields scattered out of the cavity with the relation (9). But in order to decrease the computation time, a generalized reciprocity integral [6] could be evaluated over the exchange surface 'N' to obtain the amplitude of EM field scattered at the observation point P such as:

$$E_d^{S_N}(P) = \frac{2}{F\mu_0} \int_{S_N} (\vec{E}_N^+ \wedge \vec{H}_N^- - \vec{E}_N^- \wedge \vec{H}_N^+) \cdot \hat{n} dS_c \tag{13}$$

Where:

$\vec{E}_N^+$ and $\vec{H}_N^+$ are the EM fields radiated by currents on the inner walls of the termination (section 'N') in the exchange surface 'N'

$\vec{E}_N^-$ and $\vec{H}_N^-$ are the EM fields radiated on the exchange surface 'N' by currents on the inner walls of the section '$N-1$' and equivalent currents on exchange surface '$N-1$'

The use of the segmentation principle decreases significantly the complexity of the computation. Table 1 compares complexities of IPO, S-IPO and SIPO/reciprocity methods. where K is the number of

Table 1. Comparison of computational complexity.

Method	IPO	S-IPO	S-IPO/reciprocity
Complexity	$O\left(KN^2\right)$	$O\left((2P-1)\dfrac{KN^2}{P^3}\right)$	$O\left(\dfrac{KN^2}{P^2}\right)$

iterations of the IPO method, P is the number of sections and N

is the total number of facets of the cavity. According to [15] in the S-IPO method the number of iterations required to analyze a section is equal to $\dfrac{K}{P}$ and the depth of a section may be equal to the maximum dimension of its aperture. Moreover the optimization criterion (9) can be applied in each section.

Figure 14 presents a comparison of S-IPO and S-IPO/reciprocity RCS computations with a modal method [4]. The target is a cylinder with a diameter of 30 cm and a length of 45 cm. It is divided in 2 sections (Figure 13) and 4 iterations are performed in each section. The RCS is calculated at 6 GHz, for an azimuth angle range from 0 to $50°$ with a step of $1°$, in HH polarization.
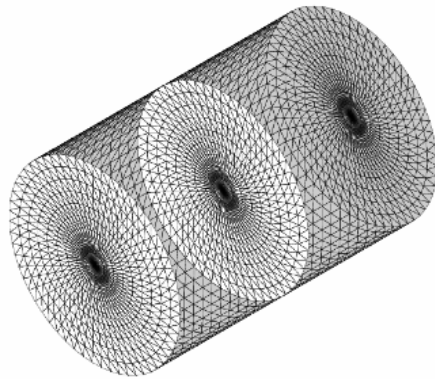
**Figure 13.** 30 cm ∗ 45 cm cylinder with 2 sections.

There is a good agreement between the three methods (Figure 14). Table 2 presents computation times on a PC with a processor of 2.8 GHz and 1 Gb of RAM.

Table 2. Cylinder RCS diagram computation times.

| Method	IPO	S-IPO	S-IPO/reciprocity
Computation times	1H10	50min	35min

Computation times are significantly reduced with the use of the S-IPO method in comparison of IPO computations and more with the use of the general reciprocity integral. IPO computation time is divided by 2 with the use of the S-IPO/reciprocity.

Then the convergence criterion is used to reduce computation times. Figure 16 and Figure 17 present comparisons of Modal Method
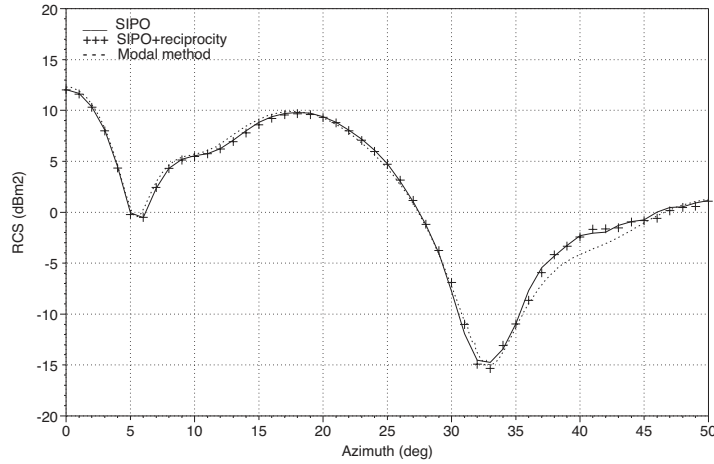
Figure 14. Comparison of S-IPO, S-IPO/reciprocity and modal method. $F = 6\,\text{GHz}$, HH polarization, elevation angle $0°$.

results with S-IPO results obtained using a convergence criterion, respectively with and without using reciprocity theorem. The target studied here is a cylinder with a diameter of 25 cm and a length of 76 cm. It is divided in 3 sections (Figure 15). S-IPO computations are performed at a 10 GHz frequency, for an azimuth angle range from $0°$ to $70°$ with a step of $2°$ and a HH polarization.
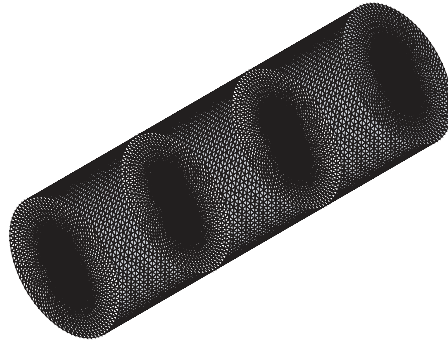

Figure 15. 25 cm $*$ 76 cm cylinder with 3 sections.

S-IPO results have a good accuracy in comparison with Modal Method results in the two cases. Computation times are significantly reduced. IPO computation time is divided by 3.5 with the use of S-IPO and a convergence criterion of 0.04, and by 5.5 with the use of
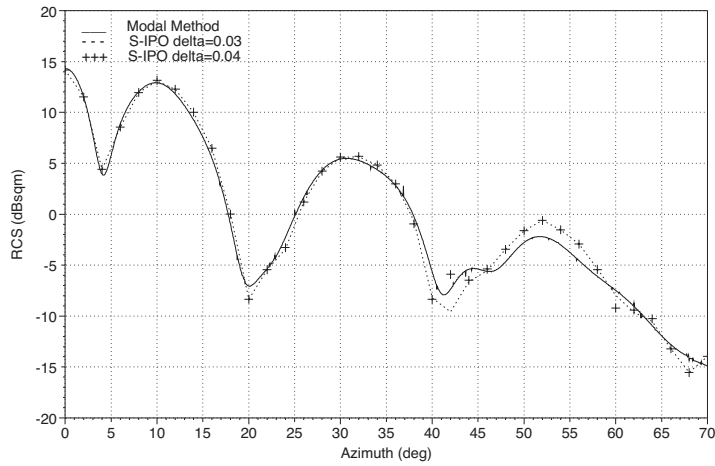
Figure 16. Comparison of Modal Method and S-IPO with convergence criterion. $F = 10\,\text{GHz}$, HH polarization, elevation angle $0°$.
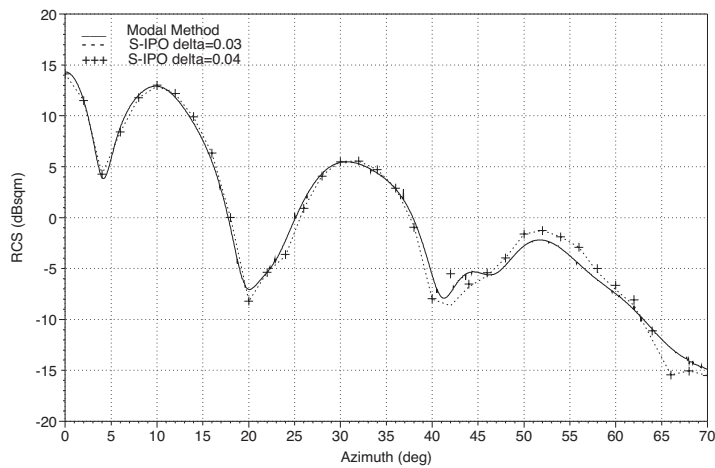
**Figure 17.** Comparison of Modal Method and S-IPO/reciprocity with convergence criterion. $F = 10\,\text{GHz}$, HH polarization, elevation angle $0°$.

S-IPO/reciprocity and convergence criterion of 0.04.

Now, we propose to study the influence of the exchange surfaces orientation and position on results' accuracy [24]. To do that, we consider the cobra cavity whose RCS has been measured in CELAR

(a)   (b)
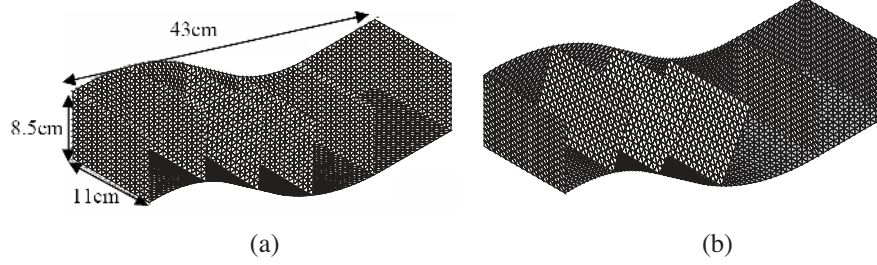
Figure 18. Orientation of exchange surfaces for the cobra cavity divided in 5 sections parallel surfaces. (a) Parallel surfaces (b) Normal surfaces.
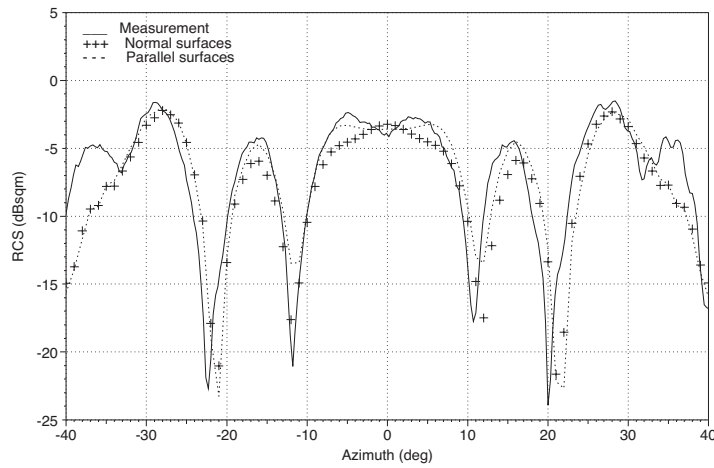
Figure 19. Cobra cavity with 5 sections, comparison of measurements with S-IPO results. $F = 16.09\,\mathrm{GHz}$, VV polarization, elevation angle $0°$.

anechoic chamber. Figure 18 shows two different orientations of exchange surfaces between sections: parallel to the open-end of the cobra cavity (Figure 18(a)) and normal to the inner walls of the cobra cavity (Figure 18(b)).

Figure 19 compares the cobra RCS computed S-IPO methods with measurements. The two configurations exchange surfaces given by Figure 18(a) and Figure 18(b) are studied. RCS is calculated at 16.09 GHz, in VV polarization, for an azimuth angle from $-40°$ to $40°$. These results show a good accuracy of S-IPO method when the Cobra is divided into 5 sections. Configuration with parallel surfaces
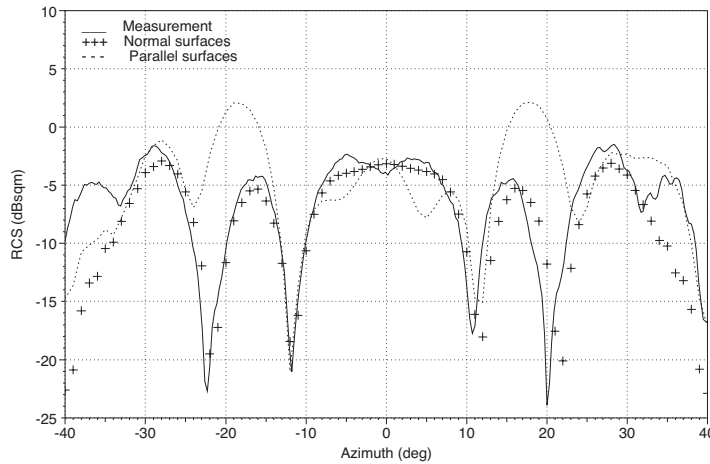
Figure 20. Cobra cavity with 4 sections, comparison of measurements with S-IPO results. $F = 16.09\,\text{GHz}$, VV polarization, elevation angle $0°$.

has a better accuracy than the one with normal surfaces. The depth of a section is approximately the same than the minimum dimension of the aperture. The same computations have been performed on the cobra divided in 4 sections with parallel and normal exchange surfaces (Figure 20). In this case the depth of a section is the same than the maximum dimension of a section. We observe that with normal exchange surfaces, S-IPO results present a good agreement with measurement. But in the case of parallel exchange surfaces, results are not good. This study shows that results obtained with exchange surfaces normal to the inner walls are better that results obtained with parallel surfaces.

Finally the repartition of electric currents density on the inner walls of the cavity and over the aperture obtained with the IPO method and S-IPO method are presented. Figure 21 and Figure 22 represent maps of electric currents on the inner walls and aperture of the cobra cavity. For S-IPO computation the cavity is divided in 5 sections with parallel exchange surface (Figure 18(a)) and the electric currents density is represented Figure 22 in the forward way. The electric currents have been represented for an azimuth angle of $30°$, an elevation angle of $0°$, a $17.5\,\text{GHz}$ frequency and a vertical polarization of the incident wave.

Few differences of electric currents on the inner walls and over the aperture of the cavity computed with IPO and S-IPO methods

are observed. These differences are mainly modifications of electric currents density distributions on the inner walls. We explain these because S-IPO method calculates currents in a sub-cavity from currents in the previous section, whereas IPO method takes into account all the cavity. Moreover Figure 22 shows weak discontinuities at exchange surfaces.

An acceleration of the IPO method based on a segmentation principle is presented. A good accuracy is obtained with this method in comparison with measurements. Computation times are significantly decreased in regard to IPO ones.

4. EVOLUTION OF THE IPO TO COMPUTE RCS OF CAVITIES WITH RADOME

In this section, an evolution of the IPO method to solve the problem of electromagnetic scattering by cavities closed by radome [23] is presented. Now the aperture is closed by a dielectric layer. Then, the Fresnel coefficients [10] are used with the IPO algorithm to take into
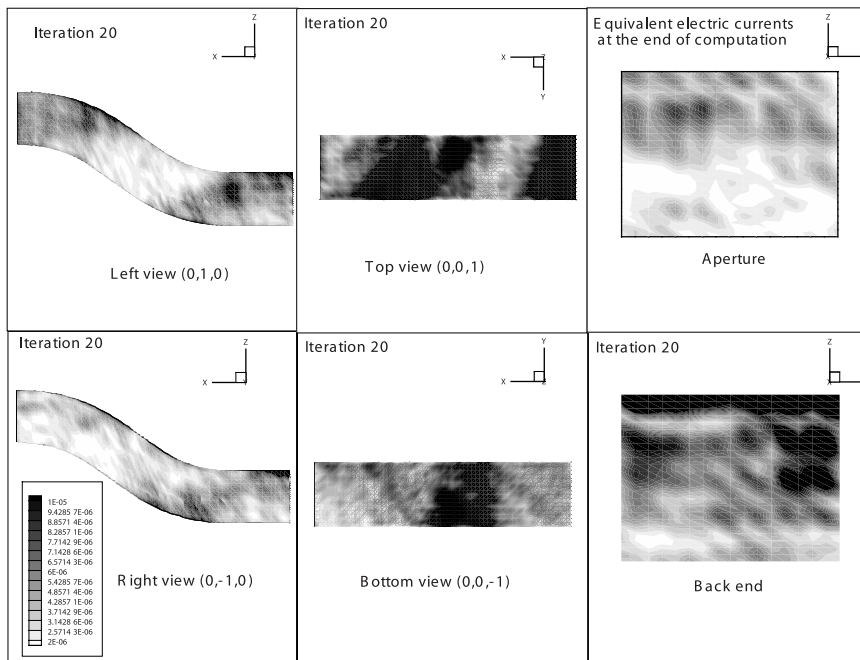
Figure 21. Electric currents density computed with the IPO method. $F = 17.5\,\text{GHz}$, VV polarization, elevation angle $0°$, Azimuth angle $30°$.
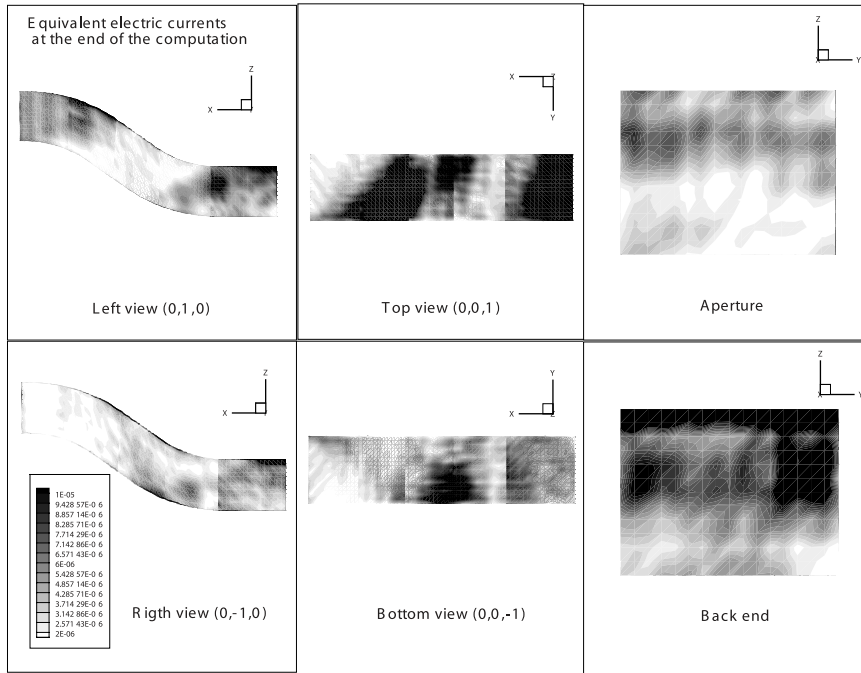
Figure 22. Electric currents density computed with the S-IPO method in the forward way. $F = 17.5\,\text{GHz}$, VV polarization, elevation angle $0°$, Azimuth angle $30°$.

account the dielectric layer characteristics. The computation algorithm is also divided in five steps as in IPO:

1. Computation of currents induced by incident EM field on the interior surface of the radome after transmission across it.

2. Computation of EM field scattered by the radome on the inner walls of the cavity.

3. Iterative computation of currents induced on each facet of the inner walls of the cavity, due to the multiple reflections on the other facets of the inner walls and the radome inner surface.

4. Computation of currents induced on the exterior surface of the radome after transmission, of EM fields scattered by the cavity inner walls, across its dielectric layer.

5. Computation of EM fields scattered outside the cavity

Equations are presented for Perfectly Electrical Conducting (PEC) cavities, but can be easily adapted to cavity with surface

impedance condition.

Step one: Computation of currents induced on the radome inner surface

These currents are computed using the Fresnel transmission coefficients [3]:

$$\vec{J}_i^T(P_a) = \hat{n}_a \wedge \vec{H}_i^T(P_a) = \hat{n}_a \wedge \left(T_H^{//} \vec{H}_i^{//}(P_a) + T_H^{\perp} \vec{H}_i^{\perp}(P_a) \right) \quad (14)$$

$$\vec{M}_i^T(P_a) = \vec{E}_i^T(P_a) \wedge \hat{n}_a = \left(T_E^{//} \vec{E}_i^{//}(P_a) + T_E^{\perp} \vec{E}_i^{\perp}(P_a) \right) \wedge \hat{n}_a \quad (15)$$

Where:

$\hat{n}_a$ is the unit normal to the radome interior at P_a

$T_H^{//}$, $T_H^{\perp}$, $T_E^{//}$, $T_E^{\perp}$ are Fresnel transmission coefficients

$\vec{E}_i^{//}$, $\vec{H}_i^{//}$, $\vec{E}_i^{\perp}$, $\vec{H}_i^{\perp}$ are normal and parallel components of EM fields

Step two: Magnetic field scattered on the inner walls of the cavity

It is computed using the Kirchhoff approximation:

$$\vec{H}_d^{S_a}(P_c) = \int_{S_a} \vec{J}_i^T(P_a) \wedge \vec{\nabla}'G(\vec{r}_c - \vec{r}_a)dS_a$$

$$-\frac{1}{jkZ_0}\vec{\nabla} \wedge \int_{S_a} \vec{M}_i^T(P_a) \wedge \vec{\nabla}'G(\vec{r}_c - \vec{r}_a)dS_a \quad (16)$$

Where:

$\vec{r}_a$ and $\vec{r}_c$ are respectively points on the radome S_a and on the inner wall S_c

$\vec{\nabla}'G$ is the gradient of the free space Green's function

Step three: iterative computation of currents induced on the inner walls

These currents are induced by EM fields scattered by the inner walls and also by the interior surface of the radome.

Consequently at iteration N electric current on S_c is given by:

$$
\vec{J}_N^{S_c}(P_{c_v}) = 2\hat{n}_{c_v} \wedge \left\{ \int\limits_{S_a} \vec{J}_N^{S_a}(P_a) \wedge \vec{\nabla}'G(\vec{r}')dS_a \right.
$$

$$
\left. -\frac{1}{jkZ_0}\vec{\nabla} \wedge \int\limits_{S_a} \vec{M}_N^{S_a}(P_a) \wedge \vec{\nabla}'G(\vec{r}')dS_a \right\}
$$

$$
+2\hat{n}_{c_v} \wedge \left\{ \int\limits_{S_c} \vec{J}_{N-1}^{S_c}(P_{c_u}) \wedge \vec{\nabla}'G(\vec{r})dS_c \right\} \tag{17}
$$

Where:

$\vec{r} = \vec{r}_{c_v} - \vec{r}_{c_u}$ is the vector between point 'u' and 'v' of S_c.

$\vec{r}' = \vec{r}_{c_v} - \vec{r}_a$ is the vector between 'v' on S_c and 'a' on S_a.

$\hat{n}_{c_v}$ is the unit normal vector to the inner wall in 'v'.

$\vec{J}_N^{S_a}$ and $\vec{M}_N^{S_a}$ are currents induced on the interior surface of the radome at iteration N. They are induced by directly incident magnetic field on the radome and by EM fields radiated by the inner walls $\vec{h}_{S_a}^{S_c}$ and $\vec{e}_{S_a}^{S_c}$.

$$
\vec{J}_N^{S_a}(P_a) = \vec{J}_i^T(P_a) + \hat{n}_a \wedge \int\limits_{S_c} \left\{ \vec{h}_{S_a}^{S_c}(P_{c_u}) + R_H^{//}\vec{h}_{S_a}^{S_c //}(P_{c_u}) \right.
$$

$$
\left. + R_H^{\perp}\vec{h}_{S_a}^{S_c \perp}(P_{c_u}) \right\} dS_c \tag{18}
$$

$$
\vec{M}_N^{S_a}(P_a) = \vec{M}_i^T(P_a) - \hat{n}_a \wedge \int\limits_{S_c} \left\{ \vec{e}_{S_a}^{S_c}(P_{c_u}) \right.
$$

$$
\left. + R_E^{//}\vec{e}_{S_a}^{S_c //}(P_{c_u}) + R_E^{\perp}\vec{e}_{S_a}^{S_c \perp}(P_{c_u}) \right\} dS_c \tag{19}
$$

Where:

$$
\vec{h}_{S_a}^{S_c}(P_{c_u}) = \vec{J}_{N-1}^{S_c}(P_{c_u}) \wedge \vec{\nabla}'G(\vec{r}_a - \vec{r}_{c_u}) \tag{20}
$$

$$
\vec{e}_{S_a}^{S_c}(P_{c_u}) = -\frac{1}{jkY_0}\vec{\nabla} \wedge \vec{J}_{N-1}^{S_c}(P_{c_u}) \wedge \vec{\nabla}'G(\vec{r}_a - \vec{r}_{c_u}) \tag{21}
$$

$R_H^{//}$, $R_H^\perp$, $R_E^{//}$, $R_E^\perp$ are Fresnel reflection coefficients on the radome
$\vec{h}_{S_a}^{S_c//}$, $\vec{h}_{S_a}^{S_c\perp}$, $\vec{e}_{S_a}^{S_c//}$, $\vec{e}_{S_a}^{S_c\perp}$ are normal and parallel components of $\vec{h}_{S_a}^{S_c}$ and $\vec{e}_{S_a}^{S_c}$.

Initially:

$$\vec{J}_0^{S_c}(P_{c_v}) = 2\hat{n}_{c_v} \wedge \vec{H}_d^{S_a}(P_{c_v}) \tag{22}$$

$$\vec{J}_0^{S_a}(P_a) = \vec{J}_i^T(P_a) \tag{23}$$

$$\vec{M}_0^{S_a}(P_a) = \vec{M}_i^T(P_a) \tag{24}$$

Step four: currents induced on the exterior surface of the radome

These currents are induced by EM fields radiated by the inner walls of the cavity. First EM fields induced by facet 'c' of the inner wall to the facet 'a' of the interior surface of the radome ($\vec{h}_d^{N_c}(P_a)$ and $\vec{e}_d^{N_c}(P_a)$) are evaluated.

$$\vec{e}_d^{N_c}(P_a) = -\frac{1}{jkY_0}\vec{\nabla} \wedge \vec{J}_N^{S_c}(P_c) \wedge \vec{\nabla}'G(\vec{r}_a - \vec{r}_c) * \Delta S_{n_c} \tag{25}$$

$$\vec{h}_d^{N_c}(P_a) = \vec{J}_N^{S_c}(P_c) \wedge \vec{\nabla}'G(\vec{r}_a - \vec{r}_c) * \Delta S_{n_c} \tag{26}$$

Where: ΔS_{n_c} is the surface of the interior facet 'c'

We deduce the currents on the exterior surface of the radome:

$$\vec{J}_T(P_a) = \sum_{c=1}^{N_c} \hat{n}_a \wedge \left\{ T_H^{//} \vec{h}_d^{N_c//}(P_a) + T_H^\perp \vec{h}_d^{N_c\perp}(P_a) \right\} + \vec{J}_i^R(P_a) \tag{27}$$

$$\vec{M}_T(P_a) = \sum_{c=1}^{N_c} \left\{ T_E^{//} \vec{e}_d^{N_c//}(P_a) + T_E^\perp \vec{e}_d^{N_c\perp}(P_a) \right\} \wedge \hat{n}_a + \vec{M}_i^R(P_a) \tag{28}$$

where $\vec{J}_i^R(P_a)$ and $\vec{M}_i^R(P_a)$ are the currents due to incident EM reflected by the radome to the observation point. They are given by:

$$\vec{J}_i^R(P_a) = \hat{n}_a \wedge \vec{H}_i^R(P_a) = \hat{n}_a \wedge \left(R_H^{//}\vec{H}_i^{//}(P_a) + R_H^\perp\vec{H}_i^\perp(P_a) \right) \tag{29}$$

$$\vec{M}_i^R(P_a) = \vec{E}_i^R(P_a) \wedge \hat{n}_a = \left(R_E^{//}\vec{E}_i^{//}(P_a) + R_E^\perp\vec{E}_i^\perp(P_a) \right) \wedge \hat{n}_a \tag{30}$$

Where: $R_H^{//}$, $R_H^\perp$, $R_E^{//}$, $R_E^\perp$ are Fresnel reflection coefficients.

Step five: electric field scattered outside the cavity

It is computed using the Kirchhoff approximation:

$$\vec{E}_d^{S_a}(P) = -\int_{S_a} \vec{M}_T(P_a) \wedge \vec{\nabla}'G(\vec{r}_p - \vec{r}_a)dS_a$$

$$-\frac{1}{jkY_0}\vec{\nabla} \wedge \int_{S_a} \vec{J}_T(P_a) \wedge \vec{\nabla}'G(\vec{r}_p - \vec{r}_a)dS_a \qquad (31)$$

This method has been validated by comparison with FEM computations. Figure 23 presents the RCS of the 12 cm∗12 cm cylinder, closed with a radome in Teflon ($\varepsilon_r = 2.1 + j0.005$, $\mu_r = 1 + j0$) and a thickness of 3 mm. The RCS is computed in VV polarization for an azimuth angle range from 0 to 50° with a step of 1° at 10 GHz and 8 iterations are performed.
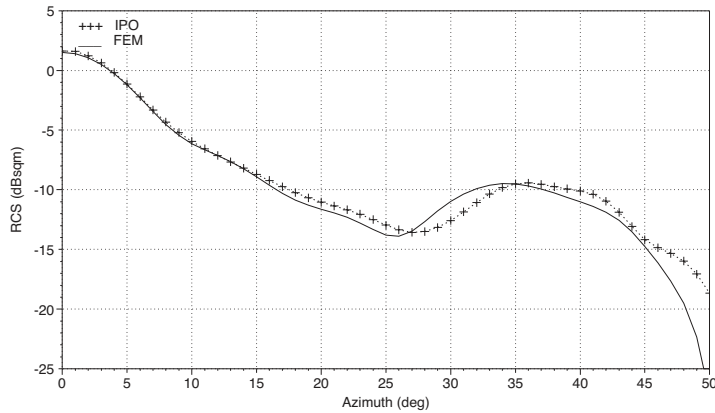

Figure 23. Comparison of FE and modified IPO methods for cavities with radome. $F = 10$ GHz, VV polarization, elevation angle 0°.

There is a very good agreement between the two methods. Then the influence of the radome on the RCS of a X band short-circuited horn (Figure 24) has been evaluated.

The RCS has been computed at 10 ghz, for an azimuth angle range from 0 to 60° with a step of 1° and in VV polarization. Three configurations are compared Figure 25: the open-ended horn, the horn with a Rohacell radome ($\varepsilon_r = 1.07 + j0$, $\mu_r = 1 + j0$) with a thickness of 3 mm and the horn with a Teflon ($\varepsilon_r = 2.1 + j0.005$, $\mu_r = 1 + j0$) radome. Observation of Figure 25 shows the radome in Rohacell has a little influence on the RCS in comparison of the open-ended horn. The radome in Teflon has more influence but the general shape of the
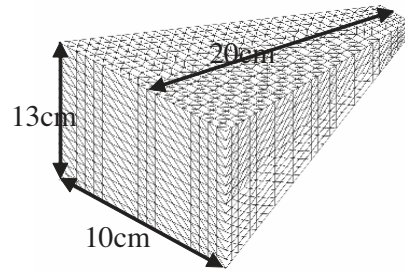
Figure 24. X band short-circuited horn.
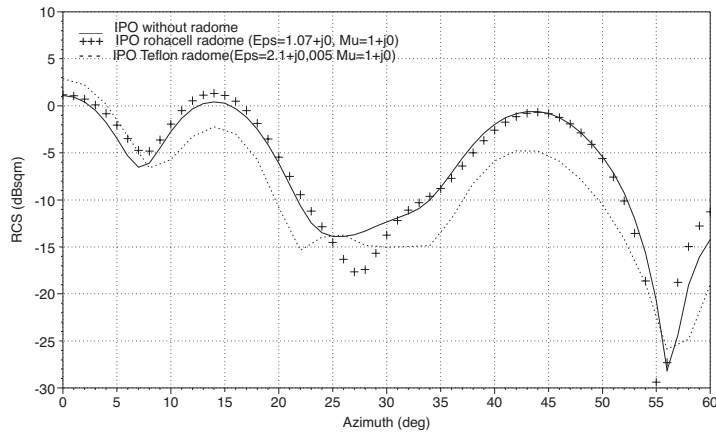
Figure 25. RCS of a X band horn with and without radome. $F = 10\,\text{GHz}$, VV polarization, elevation angle $0°$.

curves is similar. Radome in Teflon decreases the RCS for azimuth angle superior to $10°$.

5. CONCLUSION

This paper recalls the principle of the IPO method. Some comparisons of this method with measurements and other methods have been made to validate the IPO method. Comparison with measurements has shown that the IPO method is also efficient for cavities which depth is inferior to the wavelength. IPO method presents better results than Ray method in comparison with FE method especially in cross polarization. The use of a convergence criterion permits to decrease computation times. Then a new formulation of S-IPO method and the

general reciprocity integral are presented. The S-IPO method has a very accuracy in comparison with modal methods and IPO results, and S-IPO is more efficient than IPO. The use of the general reciprocity integral decreases S-IPO computation times with a good accuracy. The use of a convergence criterion also decreases computation times. Finally an evolution of the IPO method to compute RCS of cavities closed by a radome is presented and validated. In future works this method could be applied to compute RCS of aircraft's nose cone or the RCS or radiation pattern of antenna based in a cavity. One other way of investigation is to hybridize the IPO method with the FEM in order to compute the RCS of cavity with complex termination. The IPO method may be used to compute the EM fields radiated by the currents on the inner walls of the duct in the exchange surface with the termination. Then FEM may be used to compute the EM fields radiated by the termination in this exchange surface and finally the general reciprocity integral could be used to compute the EM fields scattered at the observation point.

REFERENCES

1. Anastassiu, H. T., "A review of electromagnetic scattering analysis for inlets, cavities and open ducts," *IEEE Antennas and Propagation Magazine*, Vol. 45, No. 6, 27–40, December 2003.
2. Ling, H., S. W. Lee, and R. C. Chou, "High-frequency RCS of open cavities with rectangular and circular cross sections," *IEEE Trans. Antennas Propagation*, Vol. 37, No. 5, 648–654, May 1989.
3. Altintas, A., P. H. Pathak, and M. C. Liang, "A selective modal scheme for the analysis of EM coupling into or radiation from large open-ended waveguides," *IEEE Trans. Antennas Propagation*, Vol. 36, No. 1, 84–96, January 1988.
4. He, H., "RCS prediction of cavities," Thesis for the Degree of Master Research of Electronics to Ecole Polytechnique of University of Nantes, July 2006.
5. Pathak, P. H. and R. J. Burkholder, "Modal, ray, and beam techniques for analyzing the EM scattering by open-ended waveguide cavities," *IEEE Trans. Antennas Propagation*, Vol. 37, No. 5, 635–647, May 1989.
6. Pathak, P. H. and R. J. Burkholder, "A reciprocity formulation for the EM scattering by an obstacle within a large open cavity," *IEEE Trans. Antennas Propagation*, Vol. 41, No. 4, 702–707, April 1993.
7. Burkholder, R. J., R. C. Chou, and P. H. Pathak, "Two ray

shooting methods for computing the EM scattering by large open-ended cavities," *Computer Physics Communications*, No. 68, 353–365, 1991.

8.   Ling, H., R. C. Chou, and S. W. Lee, "Shooting and bouncing rays: Calculating the RCS of an arbitrarily shaped cavity," *IEEE Trans. Antennas Propagation*, Vol. 37, No. 2, 194–205, February 1989.

9.   Syed, H. H. and J. L. Volakis, "Electromagnetic scattering by coated convex surfaces and wedges simulated by approximate boundary conditions," Ph.D. Thesis, University of Michigan, Department of Electrical Engineering and Computer Science, Ann Arbor, 1992.

10. Ruck, G. T., D. E. Barrick, W. D. Stuart, and C. K. Krichbaum, *Radar Cross Section Handbook*, Vol. 2, Chap. 7, 473–484, 1970.

11. Obelleiro, F., J. L. Rodriguez, and A. G. Pino, "A Progressive Physical Optics (PPO) method for computing the electromagnetic scattering of large open-ended cavities," *Microwave and Optical Technology Letter*s, Vol. 14, No. 3, 20 February 1997.

12. Obelleiro, F., J. L. Rodriguez, and R. J. Burckholder, "An iterative physical optics approach for analyzing the electromagnetic scattering by large open-ended cavities," *IEEE Trans. Antennas Propagation*, Vol. 43, No. 4, 356–361, April 1995.

13. Obelleiro, F., M. G. Araujo, and J. L. Rodriguez, "Iterative physical optics formulation for analyzing large waveguides with lossy walls," *Microwave and Optical Technology Letter*, Vol. 28, No. 1, 21–26, January 2001.

14. Tadokoro, M. and K. Hongo, "Measurement of RCS from a dielectric coated cylindrical cavity and calculation using IPO_EIBC," *ICEAA*, 2001.

15. Obelleiro, F., J. Campos-Niño, J. L. Rodriguez, and A. G. Pino, "A segmented approach for computing the electromagnetic scattering of large and deep cavities," *Progress In Electromagnetic Research*, PIER 19, 129–145, 1998.

16. Burkholder, R. J., "A fast and rapidly convergent iterative physical optics algorithm for computing the RCS of open-ended cavities," *ACES Journal*, Vol. 16, No. 1, March 2001.

17. Lu, C. C. and W. C. Chew, "Fast far-field approximation for calculating the RCS of large objects," *Microwave and Optical Technology Letters*, Vol. 8, No. 5, 5 April 1995.

18. Boag, A., "A Fast Iterative Physical Optics (FIPO) algorithm based on non-uniform polar grid interpolation," *Microwave and Optical Technology Letters*, Vol. 35, No. 3, 5 November 2002.

19. Boag, A., "A fast physical optics algorithm for double-bounce scattering," *IEEE Trans. Antennas Propagation*, Vol. 52, No. 1, January 2004.

20. Tokgöz, C. and C. J. Reddy, "Fast radar cross section computation by using iterative physical optics method in conjunction with adaptive model based parameter estimation," *IEEE-APS*, Albuquerque, NM, July 2006.

21. Burkholder, R. J. and T. Lundin, "Forward-backward iterative physical optics algorithm for computing the RCS of open-ended cavities," *IEEE Trans. Antennas Propagation*, Vol. 53, No. 2, 793–799, February 2005.

22. Zhang, P. F. and S. X. Gong, "Improvement on the forward-backward iterative physical optics algorithm apllied to compute the RCS of large open-ended cavities," *J. of Electromagnetic Waves and Appl.*, Vol. 21, No. 4, 457–469, 2007.

23. Hémon, R., P. Pouliguen, J. Saillard, and J. F. Damiens, "Computation of scattered fields by cavities with radome," *IEEE-APS*, Albuquerque, NM, July 2006.

24. Hémon, R., P. Pouliguen, J. Saillard, H. He, and J. F. Damiens, "Evolution and parametrical studies of IPO method," *IEEE-APS*, Honolulu, HW, June 2007.